IEEE Sensors Council

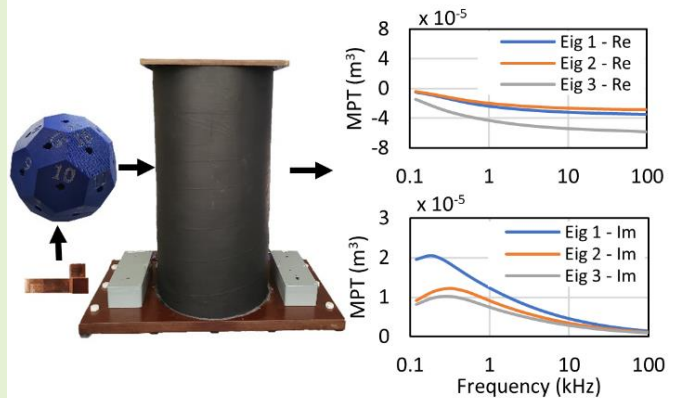# Measuring the Magnetic Polarizability Tensor of Non-Symmetrical Metallic Objects

Toykan Özdeğer, *John L Davidson, Paul D. Ledger, Daniel Conniffe,*
William R B Lionheart, Anthony J Peyton

Abstract— The Magnetic Polarizability Tensor (MPT) is a representative electromagnetic property of a metallic object, which depends on the size, material, shape, and excitation frequency of the object. The MPT can be used to describe the response of metal detector systems and improve target classification performance in applications utilizing electromagnetic induction spectroscopy. However, for target characterization, a library of possible target objects needs to be created which can be used for training machine learning classifiers. To supplement and benchmark our existing library of simulated and measured MPT object characterizations, it is necessary to be able to measure object characterizations accurately and efficiently. This paper describes a novel method utilizing a truncated icosahedron shaped manipulator and procedure to measure MPT characterizations of non-symmetrical, irregular objects. This new method allows the measurement of the MPT of any appropriately sized object. The method also ensures the MPT characterizations are measured quickly and are well posed, without sacrificing accuracy. Performance of the method is validated by comparing experiment results acquired using the new method with experiment results acquired using a slower method for symmetrical objects as well as synthetic results generated using a commercial finite element package and an optimized dedicated open source MPT-Calculator package, which offers high accuracy and considerable computational advantages. Good agreement between the new method and the other three methods is seen. For all objects that have been characterized, MPT loss-peak magnitude and horizontal positions from all described methods are within five percent of each other at worst.

Index Terms— Electromagnetic Induction Spectroscopy, Magnetic Polarizability Tensor, Metal Detection, Metal Classification

I. INTRODUCTION

The Magnetic Polarizability Tensor (MPT) is a representative electromagnetic property of a metallic object, which depends on the size, material, shape, and excitation frequency of the object. Recent progress in mathematical theory

Toykan Özdeğer, John Davidson, Daniel Conniffe, Anthony J. Peyton are with the Electrical and Electronic Engineering Department, The University of Manchester, Manchester, UK, M13 9PL (e-mail: toykan.ozdeger@manchester.ac.uk; J.Davidson-2@manchester.ac.uk; daniel.conniffe@manchester.ac.uk; a.peyton@manchester.ac.uk).
William R.B. Lionheart is with the Department of Mathematics, The University of Manchester, Manchester, UK, M13 9PL (e-mail: bill.lionheart@manchester.ac.uk).
Paul D. Ledger is with the Department of Mathematics, The University of Keele, Keele, UK (e-mail: p.d.ledger@keele.ac.uk).

has demonstrated that the MPT provides the object characterization in the leading order term of the asymptotic expansion of the perturbed magnetic field in the presence of a conducting permeable object [1]-[4]. The MPT along with Electromagnetic Induction Spectroscopy have been successfully applied in the area of metal detection e.g. the detection of unexploded ordnance [5]-[8], walk-through metal detectors [9], metal classification and recognition [10], [11], Non Destructive Testing (NDT) [12]-[14], and buried object detection [15]. MPT and broadband inductive sensing have also been previously proposed for landmine detection [16]-[24]. All these application areas have adopted some system-specific methodology to interrogate effectively the object of interest in three-dimensional space in order to calculate the MPT.

To measure the MPT of an object, its electromagnetic signature needs to be examined from several directions and with different applied field orientations. Several authors have described their system-specific methodology of experimentally determining the MPT. One particular approach is to use multiple coil arrangements. For example, the handheld sensor described in [5] uses five receive coils at different locations and

the whole sensor is moved around the target object to subject it to fields from different directions. A similar approach was taken in [6] by moving a handheld sensor (Geophex GEM-3) above the target to retrieve the MPT. However, the reported methodology only covers objects with symmetrical geometries. A non-linear inversion methodology was used in [7] by applying Gauss-Newton algorithm to data acquired from [5] and [8], where multiple coils are used. The multiple coil approach has also been used in walk-through metal detectors for determining the MPT e.g. Makkonen *et al* describes [9] a system used for object classification via determination of the spectroscopic tensor. In this case, a Levenberg–Marquardt algorithm was used to solve the optimization problem to arrive at the MPT from the Electromagnetic Induction (EMI) data where position and orientation of the target objects were not known. Another novel multiple coil arrangement has been reported in [11] which uses eight coils positioned in a circular array around the target object. The system was used for workpiece recognition by capturing electromagnetic characteristics of the target object at different angles at the same time as opposed to rotating the sensor or the object.

An alternative approach to using multiple coils is to either rotate or move the target object with respect to a known primary field thereby effectively interrogating the target in the three-dimensional field space. Scott and Larson [20], [21] describe a laboratory positioner with three automated translational stages, two automated rotational stages (yaw and pitch), and one manually adjusted roll stage. An EMI sensor array fixed to the positioner enables the measurement of the induction response of a target as a function of position. The system has been used to characterize targets such as AP landmines, rifle cartridges and steel nails and in [20] report MPT data generated using a dipole expansion and inversion technique [21] developed for the measurement of the magnetic susceptibility of soils and the polarizability of metallic objects. Objects were rotated in steps around the x-axis continuously where the rotation on other two axes were stepped once one rotation was complete around the x-axis. Each experiment lasted 19 hours caused by the large amount of data points. A least squares method was then used to arrive at the MPT characterizations of the target objects using responses from each orientation.

MPT calculation has also been applied to planar coil arrangements. Ambrus *et al* present simulated data from seven different planar coil geometries applied to test three different MPT inversion methods [15]. Optimized coil geometries ranged from single transmit and receive coil to single transmit and nine receive coils arranged in such a way as to best interrogate the target object space. Evaluated algorithms included non-linear least squares, conjugate gradient, Levenberg-Marquardt and Broyden-Fletcher-Goldfarb-Shannon (BFGS) methods applied to simulated buried cylindrical objects. Zhao *et al* [16] has also evaluated the performance of different inversion methods applied to different coil geometries and measurement protocols. Explored geometries included in-line axial scanning, multi-position measurements over a coplanar coils and target rotation within a balanced coaxial coil arrangement utilizing one transmit and two receive coils. A least squares inversion method was also applied in [17] to synthetic planar coil data to arrive at MPTs

and estimate object location in the application area of humanitarian demining. Application of a non-linear inversion method (not specified) was suggested for synthetic planar coil data taken at different locations compared to the object in [18] where the non-linearity of the problem was caused by the object's location being unknown.

Given an object's shape, size and material parameters the MPT of an object as a function of frequency (known as its spectral signature) can also be computed numerically using, for instance, the finite element method. To accelerate computations of the MPT spectral signature a proper orthogonal decomposition reduced order model with a-posteriori error estimates has been developed in the form of the open source MPT-Calculator software [25], which has been used to produce MPT spectral signatures of realistic threat objects [26] resulting in the open MPT-Library dataset. This approach employs a higher order Finite Element Method (FEM) accelerated by a reduced order model for rapid computation of the MPT spectral signatures. A comparison of different machine learning approaches has been presented in [27], with classification learnt from invariant MPT spectral signatures.

As outlined by the literature, accurate determination of the MPT depends upon many contributing factors including the sensor coil geometry, measurement protocol, acquired signal to noise level and appropriate selection of an inverse solution method. The interaction of these factors is not always well understood. Additionally, knowledge of how the target object interrogates the applied primary field space is a crucial requirement. For uniform fields and symmetrical objects this can be simplified by target rotations about simple orthogonal planes. For non-symmetrical targets, the interaction between applied field and target becomes more complex and simple rotations around orthogonal planes may either be insufficient to acquire an accurate MPT or become overly time consuming.

One of the motivations of MPT research is to develop a comprehensive library of objects in order to distinguish between threat and benign targets. For example, clutter items in post-conflict areas have a detrimental effect on the False Alarm Rate (FAR) in humanitarian demining [28]. If an MPT library of landmines and common metallic clutter found in post-conflict areas is to be constructed, landmine detectors could utilize this library to reduce FAR and speed up the demining process, especially when coupled to secondary detection such as GPR [28]. However, such a library could only be constructed with an efficient and fast method of characterizing objects.

In [22], an MPT measurement system utilizing a multi-coil arrangement with custom electronics and software is described. The system uses a wide frequency spectrum and is able to characterize large objects such as AP landmines, and landmine surrogates. However, the Target Orientation Manipulator (TOM) in [22] only rotates objects around one axis, therefore, only objects with symmetrical shape and homogeneous material distribution can be characterized, without multiple manual iterations. Consequently, we propose a new target rotational measurement protocol involving a set of orientations which are sufficient to acquire accurate MPTs.

This paper describes an efficient method utilizing a truncated icosahedron shaped TOM for characterizing MPTs of non-

symmetrical and non-homogeneous objects. Experimental data acquired using this novel TOM are compared with data acquired using the TOM in [22] for validation. The data is then further validated using synthetic data generated by a commercial FEM package and the open source MPT-Calculator simulation method described in [26].

In this paper, Section II describes the MPT, the underlying mathematical theory and how it can be related to real measurements. We also describe the geometry that we used for the TOM and why it is a well posed solution for non-symmetrical object characterization. Section III describes the experimental setup used for MPT measurement which involves the coil arrangement, system electronics, control software and the new target orientation manipulator. Section IV describes the experimental procedure followed to characterize MPT of target objects. Sections V and VI discuss the FEM and the MPT Calculator, respectively, which are used for generating synthetic data to validate experimental data. The experimental and synthetic data are then presented and compared in Section VII to prove the method's performance. Finally, Section VIII concludes the paper with a discussion of the experimental method's potential and further work.

II. BACKGROUND

A. Magnetic Polarizability Tensor

Our interest lies in characterizing hidden conducting permeable objects when the eddy current approximation of the Maxwell system, i.e. when the excitation frequency ω is small and conductivity σ_* of an object high (a more formal definition also involves the shape of the object [29] and its magnetic permeability μ_*,). Given orthonormal coordinate basis vectors $\boldsymbol{e}_i$, $i = 1,2,3$, the complex symmetric rank 2 magnetic polarizability tensor (MPT)

$$\mathcal{M} = (\mathcal{M})_{ij} \boldsymbol{e}_i \otimes \boldsymbol{e}_j, \tag{1}$$

which is a function of the object's shape, its size α as well as $\mu_*, \sigma_*, \omega,$ has been shown to provide object characterization information in the leading order term of an asymptotic expansion of the perturbed magnetic field in the form

$$(\boldsymbol{H}_\alpha - \boldsymbol{H}_0)(\boldsymbol{x})_i = \left(\boldsymbol{D}_x^2 G(\boldsymbol{x}, \boldsymbol{z})\right)_{ij} (\mathcal{M})_{jk} \left(\boldsymbol{H}_0(\boldsymbol{z})\right)_k + \boldsymbol{R}(\boldsymbol{x})_i \tag{2}$$

as $\alpha \to 0$. In the above, $G(\boldsymbol{x}, \boldsymbol{z}) = 1/(4\pi|\boldsymbol{x} - \boldsymbol{z}|)$ denotes the free space Laplace Green's function, $\boldsymbol{H}_0(\boldsymbol{z})$ the background field at the position of the object and $\boldsymbol{R}(\boldsymbol{x})$ a residual term with a known form, as shown by Ledger and Lionheart [1]-[4]. Furthermore, in these works, Ledger and Lionheart give several different equivalent expressions for computing $(\mathcal{M})_{jk}$ as a post-processing step once a vector valued transmission problem has been solved and explain its mathematical properties, including its behavior with ω.

In [2] Ledger and Lionheart explain the connection between (2) and the perturbed voltage measured by a metal detector for several practical scenarios. In the case of small coils placed a long way from the metal detector, the perturbed voltage is in the form $\boldsymbol{m} \cdot (\boldsymbol{H}_\alpha - \boldsymbol{H}_0)(\boldsymbol{x})$ where $\boldsymbol{m}$ is the dipole moment of the measurement coil, while, for larger coils placed close to the object, then integrals of the form

$$\int_S \boldsymbol{n} \cdot (\boldsymbol{H}_\alpha - \boldsymbol{H}_0)(\boldsymbol{x}) \, \mathrm{d}\boldsymbol{x} \tag{3}$$

over appropriate cross-sectional surfaces of measurement coils with unit normal $\boldsymbol{n}$ predict the perturbed voltage. In both cases the perturbed voltage can be shown [2] to reduce to the form

$$\Delta V = \boldsymbol{H}_0^{Ms}(\boldsymbol{z}) \cdot (\mathcal{M} \boldsymbol{H}_0^{Tr}(\boldsymbol{z})) \tag{4}$$

where $\boldsymbol{H}_0^{Ms}(\boldsymbol{z})$ is the background field at the position of the object that would result if the measurement coil(s) is used an excitor and $\boldsymbol{H}_0^{Tr}(\boldsymbol{z}) = \boldsymbol{H}_0(\boldsymbol{z})$ is the background field resulting from the transmitting coil at the position of the object.

B. Truncated Icosahedron

The MPT has at most 6 independent complex coefficients and transforms under rotation as

$$(\mathcal{M})_{ij} = (\mathrm{R})_{ip}(\mathrm{R})_{jq}(\mathcal{M})_{pq} \tag{5}$$

where R is the orthogonal rotation matrix describing the object transformation. To determine the MPT coefficients $(\mathcal{M})_{ij}$, it is important that measurements of ΔV are made at sufficiently many, appropriately chosen rotations of the object. Just choosing 6 randomly chosen rotations is not guaranteed to fully determine $(\mathcal{M})_{ij}$ unless the directions are independent. Furthermore, in order minimize measurement errors, many more than 6 directions and measurements are preferred. To ensure consistency and accuracy of measurements, as well as to accelerate MPT measurements, an approach whereby the rotations of the object can always be guaranteed to be the same is desired.

A truncated icosahedron (tI) [30], [31] as shown in Fig. 1 is an Archimedean polyhedral solid object with 32 faces comprising of 12 regular pentagons and 20 regular hexagons. Many will recognise the pattern of faces as being the same as used in a traditional football (soccer ball in the U.S.). The pentakis dodecahedron [32] is the dual polyhedron of the tI, the vertices of the former being projections of the face centres of the truncated icosahedron. For the unit case, these vertices are defined in Cartesian coordinates given by 12 cyclic permutations each of $(0, \pm1, \pm\varphi)$ and $(\pm\varphi, \pm1/\varphi, 0)$ and eight points defined by $(\pm1, \pm1, \pm1)$ where φ is the golden ratio [33]. It is trivial to use these coordinates to define azimuth and polar angles of a conventional spherical coordinate system to define 32 rotation matrices (with one being the identity matrix) that reorientate the tI from a conical choice with *face 1* at its base, say, to situations where each of its other 31 faces are at its base. Importantly, these 32 orthogonal rotation matrices should be distinguished from the orthogonal matrices, which make up the rotation group and symmetry group of a tI, which have orders 60 and 120, respectively. In the case of rotation group, these comprises of the 60 rotation matrices for which the configuration of the tI is preserved. The symmetry group additionally includes the 60 orthogonal matrices corresponding to the tI symmetries.

We fix an object in the centre of a hollow tI so if the tI is rotated then the object will also be rotated by the same amount. By numbering the faces of the tI, it becomes a simple matter to manually reorientate the tI and, hence the object, according to each of the face of the tI. The flat faces of the tI reduces considerably the uncertainty in the rotations, as explicit rotation

matrices are known that reorientate the tI according to its different faces. Additionally, if an object is positioned in the center of the tI, then we can use the symmetry of $\mathcal{M}$ and the form of (4) to reduce the number of faces that need to be considered from 32 to 16 as follows. Considering two opposite faces of the tI, with centers $f_n = -f_{n+16}$, their associated orthogonal reflection matrix is R = −I, where I is the identity matrix. Then, using (5), $\mathcal{M}' = \mathcal{M}$ and, hence, opposite faces do not provide additional information. For other non-opposite faces, the Rodriguez rotation formula can be used to obtain the orthogonal rotation matrix R between faces, which, using (5), leads to $\mathcal{M}' \neq \mathcal{M}$ for a general object. This information, together with form of the measurements in (4), can be used to build an overdetermined system of linear equations for the 6 unknown MPT coefficients at each frequency, which is solved using least squares. The use of the tI thereby guarantees that the directions are independent and provide a simple method to ensure consistency and accuracy of the directions and orientations used for the measurements.
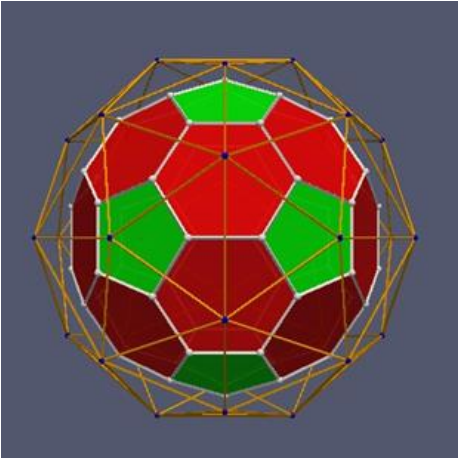

Fig. 1. The truncated icosahedron shown with red hexagon and green pentagon faces within its dual polyhedron shape of the pentakis dodecahedron represented as a wire frame.

III. EXPERIMENTAL SETUP

A. System Overview

A description of the main system used was previously published in [22], which consists in three main parts: a control software on a PC, system electronics, and a coaxial coil arrangement. The control software communicates with the microcontroller of the system electronics bidirectionally by sending signals to control the output amplitude, frequency, data acquisition settings, and receiving the measured transimpedance between transmit and receive coils. Post-processing of the data is also done by the control software, which outputs MPT eigenvalues. The system is designed to be used in a laboratory setting and aims to provide accurate and consistent MPT measurement of metal objects.

The microcontroller (Red Pitaya – STEMlab 125-14) sends excitation signals to 20 transmit amplifiers according to the experiment settings and acquires signals from two input amplifiers, one for receive coil voltage and one for transmit coil current. Half of the transmit amplifiers are configured as

inverting, while the rest are as non-inverting. The transmit amplifier circuit can provide a 64 V sine wave output at 10 A.

The coaxial coils shown in Fig. 2 consists of an outer transmit coil (240 mm in diameter), made up of nine individual sections, and two inner identical receive coils (220 mm in diameter) connected in series opposition, each made up of four individual coil sections. The coils were designed using Helmholtz coils principle and the application of the Biot-Savart Law to achieve a uniform magnetic field inside the coils. There is a two-turn current pick-up coil placed at the bottom of the coil arrangement, which acts as the current sensor of the system. Overall height of the coil arrangement is 500 mm.
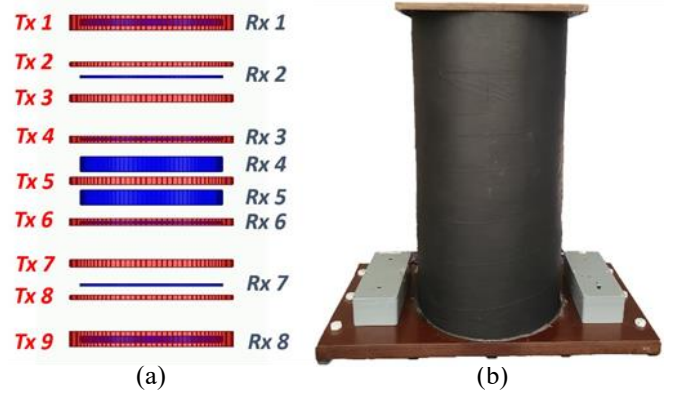

(a) (b)

Fig. 2. The coil arrangement. (a) showing alignment of the coils and (b) showing the constructed coil arrangement [22].

B. Target Orientation Manipulator

A custom-built, tI shaped target orientation manipulator (TOM) shown in Fig. 3 is used to rotate objects in three-dimensional space. The TOM is 3D printed using polylactic acid (PLA) filament and has a diameter of 150 mm and a 10 mm wall thickness. As target objects can be rotated around all three axes using this method, objects without symmetrical geometries and homogeneous materials can be characterized. Each face of the TOM has a keyed hole in the middle. These -
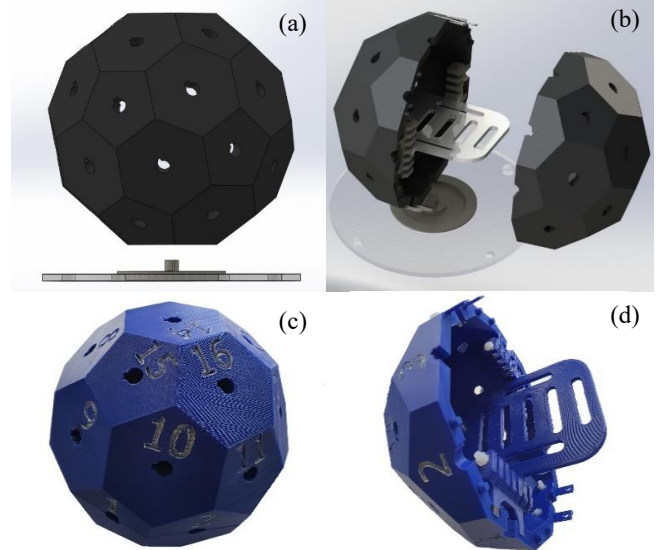

Fig. 3. Computer Aided Design (CAD) models and built version of the Target Orientation Manipulator. (a) and (c) showing closed CAD and built versions. (b) and (d) showing CAD and built versions.

are used to place the faces on a custom-made table with a keyed seat, which helps control the horizontal position and keeps rotation around the vertical axis fixed for consistency. The manipulator is built in two halves to allow access to the internal object mounting plate. Vertical position of the mounting plate can be adjusted to ensure the target object is centralised on the vertical axis of the manipulator. Target objects are securely fixed in the TOM using a combination of adhesive tape and adhesive putty.

IV. METHOD

The experimental setup was as described in our previous paper referenced in [22]. The system was set up and left running for at least half an hour before an experiment to ensure a steady-state system temperature was reached. Additionally, all experiments were done in a temperature-controlled area to minimize any potential measurement drift caused by system temperature variation. At the start of each experiment, measurements were taken with no object present in the coils to serve as a background reference. This was stored and subtracted from the measurements acquired with the target object in the coils. Phase correction was then done by using a NiZn ferrite rod as a pure real (reactive) response is expected across the operating frequency spectrum. The required correction values were then stored and applied to all subsequent measurements with target objects in the coils. MPT characterization of a target object was acquired by placing the target object inside the TOM and rotating it by placing the TOM in turn on each of its 16 faces thereby giving 16 unique and independent object orientations. Additionally, the background was measured after every two target orientations to further minimize any experimental error due to measurement drift. MPT characterization of each object was then calculated by the control software and presented in the form of MPT eigenvalues. The target objects are shown in Fig. 4. All objects were CNC machined from copper stock material to a tolerance better than 50 microns.
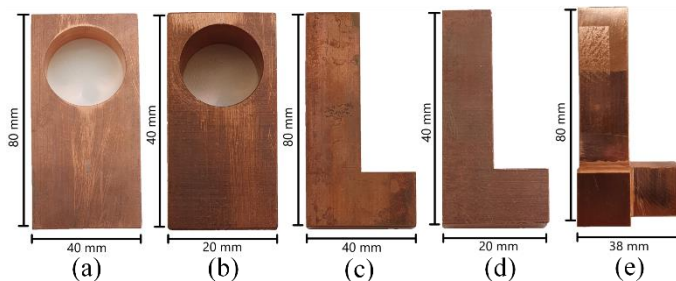

Fig. 4. Example target objects showing copper cuboid with a hole, 'L' shape and three legged 'L' shape. Object (a) and (b) copper cuboids with a hole, (c) and (d) copper 'L' shapes, (e) three legged 'L' shape. All five objects have a thickness of 10 mm where the three legged 'L' shape's third leg is 19 mm.

V. FINITE ELEMENT METHOD

Simulations were performed using the commercial FEM (Finite Element Method) solver, *Maxwell*, (*Ansys Electromagnetics Suite, Release 19.2*). The simulation geometry comprised of an outer free-space region and a three-dimensional simplified model of the segmented coil arrangement as described in [22]. Test objects were modelled

using a commercial CAD package prior to importing into the Ansys Electromagnetics suite and the modelled coil geometry. Simulations for comparison with experimental measurements involved positioning each target within the uniform field region of the modelled coils at defined angular orientations in relation to the normals of the central faces of the truncated icosahedron described in Section IIB. Polar and azimuth angles of a spherical coordinate system as shown in Fig. 5(a) were used to describe the target under test. Simulations were carried out for the 16 independent face-defined truncated icosahedron orientations of each test object. Fig. 5(b) shows an example orientation of a test object within a detailed part of the modelled coil arrangement. Each target orientation involved simulations over the frequency sweep range of 100 Hz to 100 kHz in ten logarithmic increments per decade. All test objects were modelled using a conductivity of pure copper defined as 5.8×10^7 S/m by the International Annealed Copper Standard (IACS). Typical meshing involved a FEM model of approximately 150k tetrahedral elements in total per orientation geometry with between 15k to 25k elements per test object.
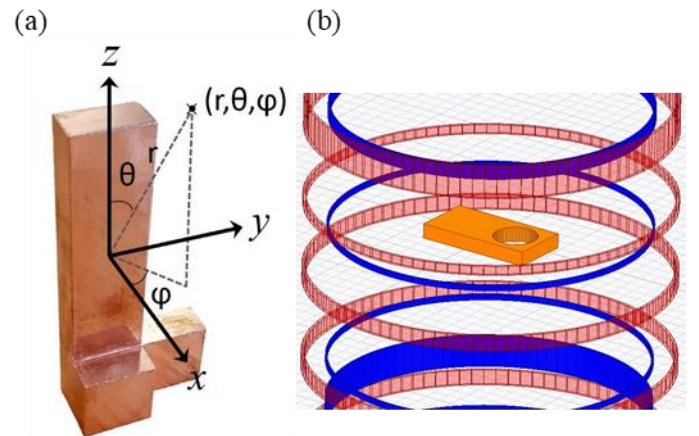

Fig. 5. FEM modelling of test objects showing (a) adopted orientation coordinate system and (b) example test object within the coil geometry at one of the independent face-defined truncated icosahedron orientations.

VI. MPT-CALCULATOR

The MPT calculator software employs the NGSolve FEM library [34]-[36] to provide accurate high-order finite element solutions to vectorial transmission problems from which the MPT coefficients $(\mathcal{M})_{ij}$ follow in a post-processing step [3]. To accelerate the computation of the MPT spectral signature, which would otherwise require full FEM solves for each frequency of interest, a reduced order model (ROM) is employed to predict the full signature from a small number of solution snapshots at different frequencies at reduced computational cost. The reduced order model benefits from a-posteriori error estimates, which the MPT spectral signature predicted by the ROM with respect to signature that would be obtained from full FEM solves at each frequency. For full details see [25].

VII. RESULTS

MPTs of various objects were measured using the new target orientation manipulator. The results were compared with MPTs

acquired from FEM simulations, MPT calculator software, and measurements that used the previous TOM. Because MPTs are object specific, the other methods were used as a verification of the new method's ability to characterize MPTs of objects correctly.

Fig. 6 shows the MPT of a copper disk, which is compared with FEM simulations and measurements from the previous TOM. Fig. 7 shows measured target objects compared with FEM simulations, measurements done with the previous TOM and values from the MPT Calculator algorithm. Fig. 8 shows

MPT of a copper 'L' shape with a third leg where all three legs are at different lengths. This makes it the most non-symmetrical object between the ones interrogated in this paper with six independent MPT coefficients.

There is a good agreement between experimental results acquired using the new and previous TOMs. For all target objects in both Fig. 6 and Fig. 7, data acquired using the new TOM, labelled as Expt 2, follow a similar curve with data -

TABLE I
NRMSE of differences between measured MPT eigenvalues compared to MPT eigenvalues generated using the MPT-Calculator algorithm.

	MPT-Calculator vs. New TOM						*MPT-Calculator vs. Previous TOM*					
	Eigenvalue 1		Eigenvalue 2		Eigenvalue 3		Eigenvalue 1		Eigenvalue 2		Eigenvalue 3	
	Re	Im	Re	Im	Re	Im	Re	Im	Re	Im	Re	Im
Small 'L' Shape	0.033	0.024	0.022	0.015	0.029	0.018	0.035	0.040	0.025	0.029	0.027	0.030
Large 'L' Shape	0.027	0.029	0.032	0.029	0.026	0.024	0.023	0.035	0.030	0.038	0.023	0.034
Small Cuboid with Hole	0.027	0.015	0.022	0.014	0.018	0.024	0.024	0.027	0.020	0.027	0.021	0.033
Large Cuboid with Hole	0.025	0.049	0.022	0.027	0.024	0.024	0.025	0.054	0.019	0.031	0.020	0.026
Three Legged 'L' Shape	0.024	0.036	0.030	0.032	0.025	0.040	N/A	N/A	N/A	N/A	N/A	N/A

TABLE II
NRMSE of differences between measured MPT eigenvalues compared to MPT eigenvalues generated using the FEM simulations.

|	*FEM vs. New TOM*						*FEM vs. Previous TOM*					
	Eigenvalue 1		Eigenvalue 2		Eigenvalue 3		Eigenvalue 1		Eigenvalue 2		Eigenvalue 3	
	Re	Im	Re	Im	Re	Im	Re	Im	Re	Im	Re	Im
Small 'L' Shape	0.046	0.062	0.028	0.054	0.031	0.053	0.048	0.078	0.031	0.064	0.031	0.062
Large 'L' Shape	0.030	0.071	0.056	0.088	0.039	0.083	0.028	0.080	0.054	0.096	0.037	0.093
Small Cuboid with Hole	0.024	0.071	0.032	0.067	0.030	0.057	0.024	0.077	0.032	0.078	0.035	0.067
Large Cuboid with Hole	0.027	0.105	0.049	0.120	0.055	0.123	0.028	0.110	0.045	0.126	0.050	0.124
Three Legged 'L' Shape	0.035	0.078	0.060	0.087	0.030	0.105	N/A	N/A	N/A	N/A	N/A	N/A
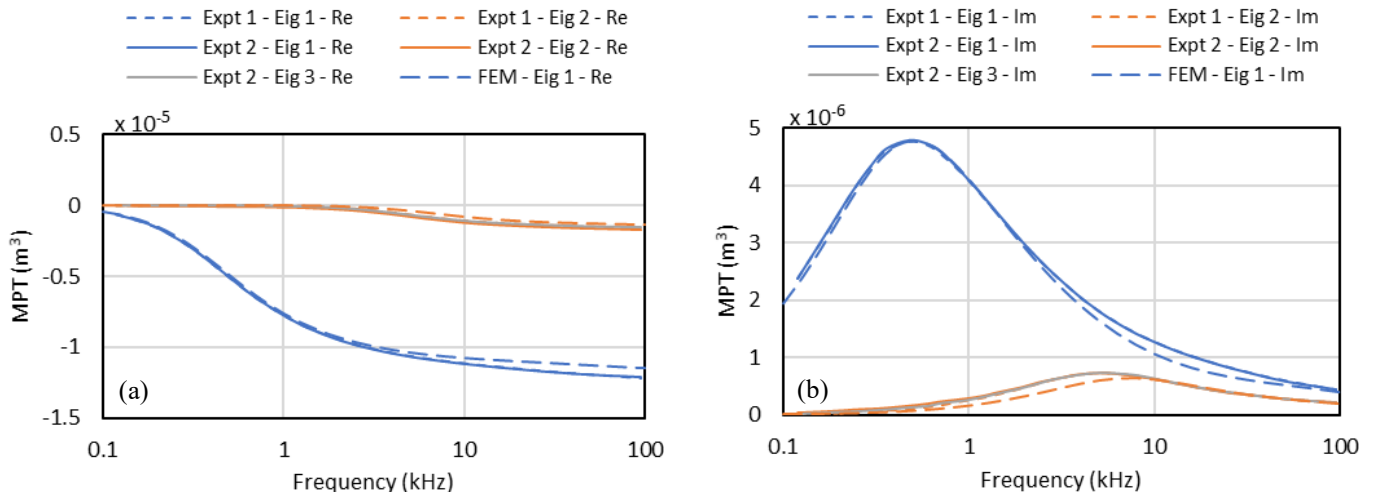
Fig. 6. Real and imaginary MPT eigenvalues for a copper disk with 30 mm in diameter and 2.15 mm thickness measured using the new object orientation manipulator, compared with measurements using previous object orientation manipulator and FEM simulations. "Expt 1" represents values from experiments done using the previous TOM while "Expt 2" represents values taken using the new one. "FEM" represents values from FEM simulations. Plots show (a) real and (b) imaginary MPT eigenvalues.
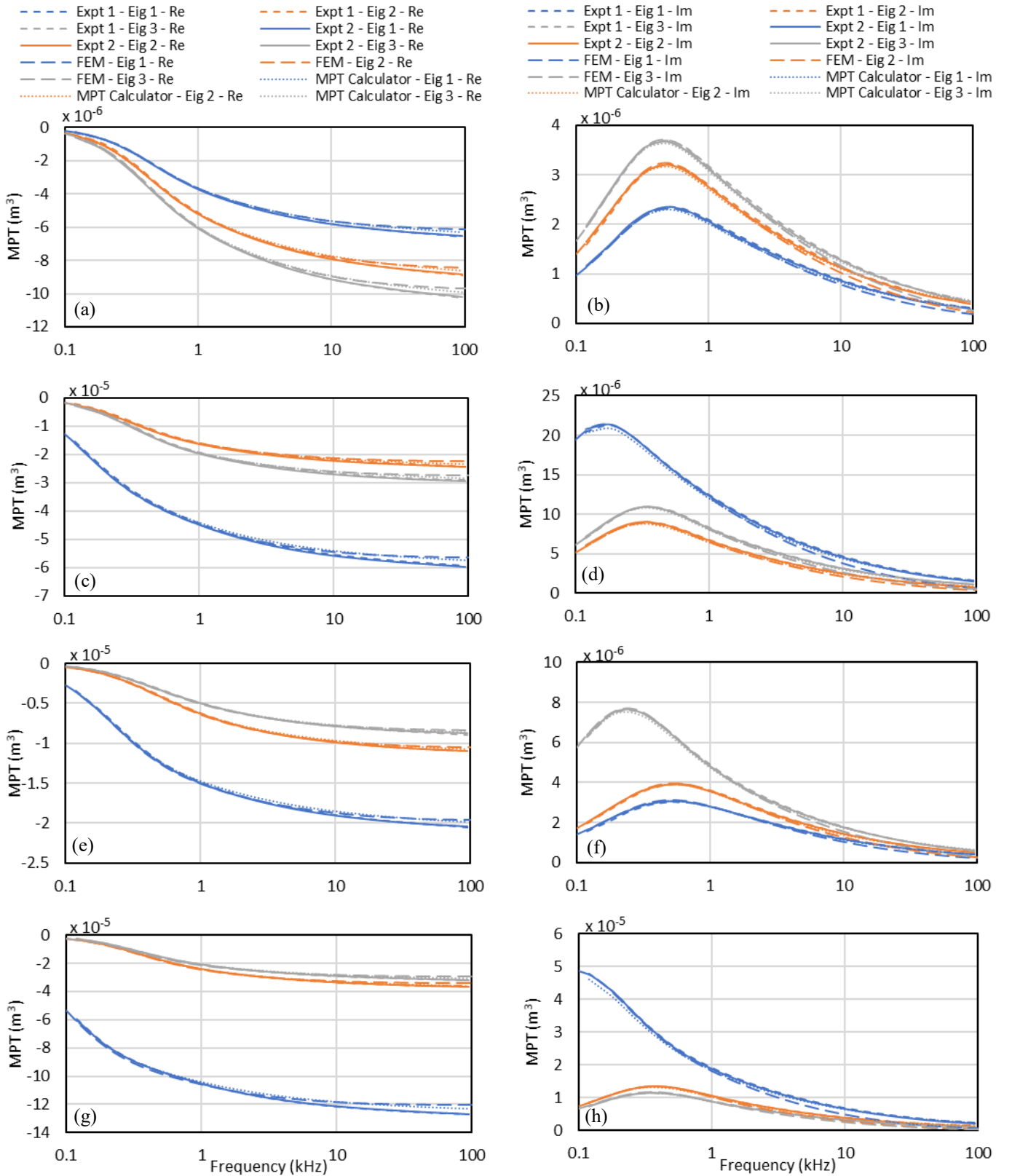
Fig. 7. Measured real and imaginary MPT eigenvalues of target objects, compared with results from FEM simulations, MPT Calculator and measurements using the previous TOM. Plots (a-b) small 'L' shape, (c-d) large 'L' shape, (e-f) small cuboid with hole, (g-h) large cuboid with hole. "Expt 1" represents values from experiments done using the previous TOM while "Expt 2" represents values taken using the new one. "FEM" represents values from FEM simulations while "MPT Calculator" represents values acquired using the MPT Calculator.
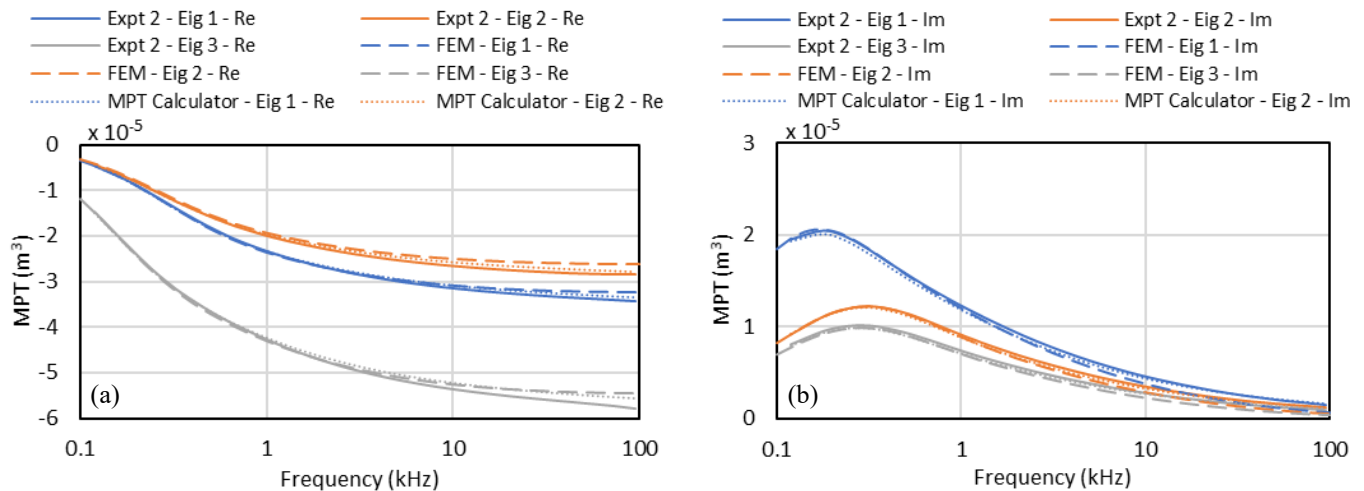
Fig. 8. Real and imaginary MPT eigenvalues for a three legged 'L' shape measured using the new object orientation manipulator, compared with results from FEM simulations and MPT Calculator. "Expt 2" represents values taken using the new TOM. "FEM" represents values from FEM simulations while "MPT Calculator" represents values acquired using the MPT Calculator. Plots show (a) real and (b) imaginary MPT eigenvalues.

acquired using the previous TOM, labelled as Expt 1. Loss-peak magnitude and horizontal positions are within less than one percent of each other. In addition, for all target objects shown in Fig. 7 and Fig. 8, MPT loss-peak magnitude and horizontal positions for new and previous TOMs, FEM simulations and MPT Calculator are within five percent of each other at worst.

The main source of error between the data from new and previous TOMs is the orientation accuracy of the previous TOM, which is around 1 degree, whereas we estimate the new TOM's orientation accuracy to be better than 1 degree. The error in orientation of an object when placed on the previous TOM also contributes to errors, as objects are not 100% symmetrical and perfectly homogeneous materials. However, these errors do not matter for the new TOM methodology, as the objects are characterized in all three dimensions. In addition to the previous approach being unable to characterize non-symmetrical objects where principal axes of the object are not obvious, it is also less accurate compared to the new TOM method when the principal axes are obvious. This is quantified in TABLE I and TABLE II, where Normalised Root Mean Square Error (NRMSE) between data generated by MPT-Calculator algorithm and FEM simulations are compared with experimental data acquired by using both TOMs. For all target objects considered in TABLE I and TABLE II, NRMSE values for data acquired using the new TOM are generally lower than the previous TOM, meaning that the new method is more accurate. NRMSE has previously been used as an analysis method for results comparison and has been described in more detail in [22], [37].

VIII. CONCLUSION AND FUTURE WORK

A truncated icosahedron shaped target orientation manipulator was designed and constructed for fast and accurate measurement of MPT characterizations. The manipulator was tested in a previously built and reported system which the performance is known. Modifications were made on the post-processing algorithm to take the rotation matrices between truncated icosahedron's faces into account. Experimental results acquired using the new target orientation manipulator methodology was compared with previously reported experimental results as well as synthetic data acquired using FEM and custom MPT-Calculator algorithms. This verified the method's ability to measure MPT characterizations of non-symmetrical, irregular metal objects accurately. The novelty of the new method is the truncated icosahedron shaped target orientation manipulator combined with the required measurement system and processing algorithms, making it a complete, measurement ready system capable of measuring rank-2 MPT characterizations. We hope to report results from this system on targets of interest for applications including humanitarian demining and security screening in the near future.

IX. REFERENCES

[1] Ledger, PD., and Lionheart, WRB., "Understanding the magnetic polarizability tensor," *IEEE Transactions on Magnetics*, vol. 52. No. 5, pp. 1-16, 2016.

[2] Ledger, PD., and Lionheart, WRB., "An Explicit Formula for the Magnetic Polarizability Tensor for Object Characterization," *IEEE Transactions on Geoscience and Remote Sensing*, vol. 56, no. 6, pp. 3520-3533, 2018.

[3] Ledger, PD., and Lionheart, WRB., "The spectral properties of the magnetic polarizability tensor for metallic object characterisation," *Mathematical Methods in the Applied Sciences*, vol. 43, no. 1, pp. 78-113, 2019.

[4] Ledger, PD, Lionheart, WRB., "Generalised magnetic polarizability tensors," *Mathematical Methods in the Applied Sciences*, vol. 41, pp. 3175– 3196, 2018.

[5] Fernandez, JP., Barrowes, BE., Grzegorczyk, TM., Lhomme, N., O'Neill, K., and Shubitidze, F., "A Man-Portable Vector Sensor for Identification of Unexploded Ordnance," *IEEE Sensors Journal*, vol. 11, no. 10, pp. 2542-2555, 2011.

[6] Norton SJ., and Won, IJ., "Identification of buried unexploded ordnance from broadband electromagnetic induction data," *IEEE Transactions on Geoscience and Remote Sensing*, vol. 39, no. 10, pp. 2253-2261, 2001.

[7] Grzegorczyk, TM., Barrowes, BE., Shubitidze, F., Fernandez, JP., and O'Neill, K., "Simultaneous Identification of Multiple Unexploded Ordnance Using Electromagnetic Induction Sensors," *IEEE Transactions on Geoscience and Remote Sensing*, vol. 49, no. 7, pp. 2507-2517, 2011.

[8] Nelson, HH., and McDonald, JR., "Multisensor towed array detection system for UXO detection," *IEEE Transactions on Geoscience and Remote Sensing*, vol. 39, no. 6, pp. 1139-1145, 2001

[9] Makkonen, J., Marsh, L., Vihonen, J., Järvi, A., Armitage, D., Visa, A. and Peyton, A., "KNN classification of metallic targets using the magnetic polarizability tensor," *Measurement Science and Technology*, vol. 25, no. 5, pp. 055105, 2014.

[10] O'Toole, M., Karimian, N. and Peyton, A., "Classification of Nonferrous Metals Using Magnetic Induction Spectroscopy," *IEEE Transactions on Industrial Informatics*, vol. 14, no. 8, pp. 3477-3485, 2018.

[11] Tao, Y., Yin, W., Zhang, W., Zhao, Y., Ktistis, C., and Peyton, AJ., "A Very-Low-Frequency Electromagnetic Inductive Sensor System for Workpiece Recognition Using the Magnetic Polarizability Tensor," *IEEE Sensors Journal*, vol. 17, no. 9, pp. 2703-2712, 2017.

[12] García-Martín, J., Gómez-Gil, J. and Vázquez-Sánchez, E., "Non-Destructive Techniques Based on Eddy Current Testing," *Sensors*, vol. 11, no. 3, pp. 2525-2565, 2011.

[13] Daura, L., Tian, G., Yi, Q. and Sophian, A., "Wireless power transfer-based eddy current non-destructive testing using a flexible printed coil array," *Philosophical Transactions of the Royal Society A: Mathematical, Physical and Engineering Sciences*, vol. 378, no. 2182, p. 20190579, 2020.

[14] Lu, M., Meng, X., Huang, R., Chen, L., Tang, Z., Li, J., Peyton, A. and Yin, W., "Determination of Surface Crack Orientation Based on Thin-Skin Regime Using Triple-Coil Drive–Pickup Eddy-Current Sensor," *IEEE Transactions on Instrumentation and Measurement*, vol. 70, pp. 1-9, 2021.

[15] Ambrus, D., Vasic, D. and Bilas, V., "Comparative Study of Planar Coil EMI Sensors for Inversion-Based Detection of Buried Objects," *IEEE Sensors Journal*, vol. 20, no. 2, pp. 968-979, 2020.

[16] Zhao, Y., Yin, W., Ktistis, C., Butterworth, D. and Peyton, A., "Determining the Electromagnetic Polarizability Tensors of Metal Objects During In-Line Scanning," *IEEE Transactions on Instrumentation and Measurement*, vol. 6, no. 5, pp. 1172-1181, 2016.

[17] Dekdouk, B., Ktistis, C., Marsh, L., Armitage, D. and Peyton, A., "Towards metal detection and identification for humanitarian demining using magnetic polarizability tensor spectroscopy," *Measurement Science and Technology*, vol. 26, no. 11, pp. 115501, 2015.

[18] Ambruš, D., Vasić, D., and Bilas, V., "Innovating on top of I&M fundamentals for safer humanitarian demining," *IEEE Instrumentation & Measurement Magazine*, vol. 23, no. 3, pp. 35-41, 2020.

[19] Dalichaouch, Y., Whitecotton, B., McManus, T., Kuhn, S., Trammell, H., Shelby, R. and Carin, L., "Wideband frequency response of low-metal mines," *Detection and Remediation Technologies for Mines and Minelike Targets IX*, vol. 5415, pp. 275-282, 2004.

[20] Scott, WR., and Larson, GD., "Modeling the measured em induction response of targets as a sum of dipole terms each with a discrete relaxation frequency," *IEEE International Geoscience and Remote Sensing Symposium*, Honolulu, HI, USA, pp. 4188-419, 2010.

[21] Larson, GD., and Scott, WR., "Automated, non-metallic measurement facility for testing and development of electromagnetic induction sensors for landmine detection," *Detection and Sensing of Mines, Explosive Objects, and Obscured Targets XIV*, 2009.

[22] Özdeğer, T., Davidson, JL., Van Verre, W., Marsh, LA., Lionheart, WRB., and Peyton, AJ., "Measuring the Magnetic Polarizability Tensor Using an Axial Multi-Coil Geometry," in IEEE Sensors Journal.

[23] Rehim, O., Davidson, JL., Marsh, LA., O'Toole, M., Armitage, D. and Peyton, A., "Measurement system for determining the magnetic polarizability tensor of small metal targets," *IEEE Sensors Applications Symposium (SAS)*, Zadar, pp. 1-5, 2015.

[24] Rehim, O., Davidson, JL., Marsh, LA., O'Toole, M. and Peyton, A., "Magnetic Polarizability Tensor Spectroscopy for Low Metal Anti-Personnel Mine Surrogates," *IEEE Sensors Journal*, vol. 16, no. 10, pp. 3775-3783, 2016.

[25] Wilson, BA., and Ledger, PD., "Efficient computation of the magnetic polarizability tensor spectral signature using proper orthogonal decomposition," *Int. J. Numer. Methods Eng.*, vol. 122, no. 8, pp. 1940–1963, 2021.

[26] Ledger, PD., Wilson, BA., Amad, AAS., and Lionheart, WRB., "Identification of metallic objects using spectral magnetic polarizability tensor signatures: Object characterisation and invariants," *Int. J. Numer. Methods Eng.*, vol. 122, no. 15, pp. 3941–3984, 2021.

[27] Wilson, BA., Ledger, PD., and Lionheart, WRB., "Identification of metallic objects using spectral magnetic polarizability tensor signatures: Object classification," *International Journal for Numerical Methods in Engineering*, Accepted Author Manuscript, 2022.

[28] Tsipis, K., "Technological Innovation in Humanitarian Demining," *Human Factors and Ergonomics Soc*, SANTA MONICA, 1998, pp. 750-753.

[29] Schmidt, K., Sterz, O., and Hiptmair, R., "Estimating the eddy-current modeling error," *IEEE Transactions on Magnetics 44*, vol. 6, pp. 686–689, 2008.

[30] Coxeter, HSM., Longuet-Higgins, MS., and Miller, JCP., "Uniform Polyhedra." *Phil. Trans. Roy. Soc. London Ser. A* 246, pp. 401-450, 1954.

[31] Cundy, H., and Rollett, A., "Stellated Archimedean Polyhedra." *Mathematical Models*, 3rd edition, pp. 123-128 and Table II following p. 144, 1989.

[32] Wenninger, M., "Dual Models," *Cambridge University Press*, MR 0730208, 1983.

[33] Catalan, E. "Mémoire sur la Théorie des Polyèdres," *Journal de l'École Polytechnique,* vol. 24, pp. 1-71, 1865.

[34] Zaglmayr, S.: PhD thesis "High Order Finite Elements for Electromagnetic Field Computation", Johannes Kepler University Linz, 2006.

[35] Schöberl, J.: "NETGEN - An advancing front 2D/3D-mesh generator based on abstract rules." *Computing and Visualization in Science,* vol. 1, pp. 41-52, 1997.

[36] Schöberl, J.: "C++11 Implementation of Finite Elements in NGSolve", *ASC Report 30/2014,* Institute for Analysis and Scientific Computing, Vienna University of Technology, 2014.

[37] Davidson, J., Abdel-Rehim, O., Hu, P., Marsh, L., O'Toole, M. and Peyton, A., "On the magnetic polarizability tensor of US coinage," *Measurement Science and Technology*, vol. 29, no. 3, pp. 035501, 2018.